Journal of Ocean Engineering and Science 7 (2022) 327–336

Contents lists available at ScienceDirect

Journal of Ocean Engineering and Science

journal homepage: www.elsevier.com/locate/joes

An improved smoothed particle hydrodynamics approach using new inverse kernel function

J.R. Rajapriyadharshini

Department of Civil Engineering, Thiagarajar College of Engineering, Madurai, TN, India

ARTICLE INFO

Article history:
Received 10 November 2020
Revised 8 September 2021
Accepted 8 September 2021
Available online 11 September 2021

Keywords:
Inverse logarithmic function
Moving least squares approximation
Shock wave propagation
3D dam-break flow
Zero error

ABSTRACT

The main limitation of Smoothed Particle Hydrodynamics (SPH) method that resists the method's potential is its lack of providing stability and accuracy to the numerical technique. We improve the accuracy of the standard SPH technique, by formulating a new inverse logarithmic kernel function. This new kernel function is derived based on the underlying properties of kernel functions. The approximation technique used here is based on the Moving Least Squares based technique. The adequacy of the proposed kernel function is tested by simulation of 2D shock wave propagation and 3D dam-break free surface flow against a cuboidal obstacle. The method was validated against experimental data by Kleefsman et al., [1]. The numerical results reveal that our new SPH approach using inverse logarithmic kernel function outperforms existing ones in particle restoration, zero error, better accuracy and enhanced efficiency in kernel approximation. This new kernel function showed some improvement over existing kernels by showing very less error approximation value of $0.035h^2$. The results showed some improvements over standard technique by being capable of handling problems with large deformations accurately and precisely.

1. Introduction

The numerical techniques have become an incredible asset in the simulation of dynamic issues in the field of material science, chemistry, biology and engineering sciences. This topic plays a pivotal role in the assessment of hypothesis, offering bits of knowledge to complex physics, and aiding the understanding and the disclosure of new wonders of science. Over the years, non-linear breaking wave impact and the development of vortices and eddy currents are modeled using Computational Fluid Dynamics (CFD) based technique. In an attempt to comprehend the fluid dynamic problems, real-time laboratory experiments were carried out on scaled models, however, these experiments experienced the ill effects of scaling issues. This has results in the introduction of further innovative numerical methods for the solution of complex fluid dynamic equations.

Smoothed Particle Hydrodynamics (SPH) uses smoothed particles or points as interpolation points in order to represent the materials at different locations. This method provides easy tracing of free surfaces, interfaces as well as moving boundaries. As SPH uses particles as computational frame rather than mesh to interpolate, it overcomes the difficulties due to significantly larger deformations. The combination of the advantages of strong form formulation like computational efficiency and the advantages of weak form formulation like stability and accuracy, adds mixed features to SPH. The stability and accuracy are due to the smoothing operator used in SPH which is represented in the integral form. This smoothing function solves in a partitioned manner iteratively. In the last decade, it is identified that SPH, a mesh-free particle method based on Lagrangian approach is being honed to solve fluid-structure interaction problems.

SPH was invented [2] and developed [3] for evaluating astrophysical problems in open space. The SPH method was then extended to solve problems of compressible flows [4,5]. Additionally, it was observed that, the smoothing function needs to be a continuous function. A good agreement with the accuracy of the method was observed when comparing Gaussian and Cubic spline kernels with the other existing kernels. Further works are carried in an extension to the previous work, where a method to construct higher order kernel functions [6] from normal kernel function was proposed. The super Gaussian kernel function was derived in that study [4]. Overall, the limitation of higher order kernel function is that it leads to unphysical results where the kernel becomes negative in part of the domain, resulting in serious consequences when there is a sharp change in density [7,8].

E-mail address: dharshini_1605@rediffmail.com

https://doi.org/10.1016/j.joes.2021.09.004

Other approaches in the SPH method to solve incompressible flows are developed [5,7–11] where the flow is treated as weakly compressible in nature. This weakly compressible nature (Weakly Compressible SPH approach) is achieved by simulating in low Mach number by selecting the smallest possible speed of sound that in addition ensures density fluctuation. The indeterminate system of equations in this approach is solving by introducing Tait's equation of state [4,12]. It is proved that SPH can be used to simulate the free surface flows, provided that the density is evaluated by approximation of its rate of change and the particles flow with corrected velocities. However, the stability and the accuracy of the method could not be evaluated.

A simulation using SPH was carried out to demonstrate the dynamic response of materials involving fracture and fragmentation [13–15]. However, the lack of the generalized boundary conditions as well as the stability, has limited the complete exploitation of the SPH method's potential [16]. Most of the existing researches state that the stability of SPH method is based on the kernel functions and is related to the second derivative of the kernel function [17]. The SPH kernel functions in one dimensional space was studied which states that the choice of kernel is a key decision before performing any calculation using SPH [18,19]. It was concluded in the same study that the cubic spline performs better than any other kernel function. Although some approaches improve the results of higher order kernel function, they do not yet address the issues of accuracy, and inconsistencies of the kernels.

A general approach to construct kernel functions was given in 2010 and a new quartic kernel function was derived in that study [20]. This new quartic kernel is validated and tested for one-dimensional shock wave and TNT detonation problems. In another study, a comparative study between the cubic spline and the new quartic kernel function was carried using lid-driven cavity problems and it has been concluded that quartic kernel gave better results than cubic spline [21]. An investigation was carried out for the purpose of avoiding confusion in selecting the kernel function [22]. In that study, the evaluation included comparison between computational accuracy of ten kernels and it has been concluded that Gaussian, and Q-spline kernels gave better results in terms of computational cost. There have been multiple previous attempts to investigate on the stability and computational efficiency of the kernel functions. A model based on harmonic function was proposed and developed, where kernels of one-parameter family are interpolated with compact supportedness [23]. This work is limited to compact supportedness property without consideration of consistency and convergence of the kernel functions. Despite the success of the earlier works on kernel function in certain aspects, it still suffers from major issues like consistency and convergence of the kernels. More recent studies on the methods of improving the accuracy and convergence of mathematical and numerical modeling like fractional iteration and variational iteration methods have been introduced [24–30]. These methods shall be used in future research to improve the efficiency of the SPH model. A comparison of all kernel functions to find the most kernel for SPH method based on consistency of the kernel was carried [14] but failed to address the accuracy of SPH method in the study. The most recent study on derivation of new double cosine kernel function was proposed and it proves that an improvement on the new proposed kernel function in terms of accuracy, and error approximation are achieved over the existing ones in the literature [31] but still the study fails to achieve zero error in the approximation.

In most of the previous research works, there are numerical drawbacks like stability, accuracy and convergence of SPH method and there come a need for the research to be carried out on the numerical analysis of the SPH method. It was further noted that although significant growth and success were achieved in SPH developments, the computational accuracy, efficiency, consistency, convergence [32] and stability need to be combined to addressed for a better solution in SPH method. A principle based on inverse kernels was given in a seminal paper [33] where higher order SPH methods are solved using inverse kernels. In keeping more closely with the spirit of Le Fang et al. [33], in this work, we attempt to derive a new kernel function based on inverse logarithmic function. The new proposed approach using inverse logarithmic function will offer an improvement on the existing SPH method in terms of stability, accuracy and error approximation. In the new proposed SPH approach, the kernels are approximated using Moving Least Squares based approximation scheme that provides better approximation of functional derivatives near the boundary particles [31,33,34].

This paper is structured as follows: SPH model design (Section 2); Kernel function for SPH (Section 3); two numerical test cases in shock wave propagation and dam break phenomena to check the ability of the improved SPH method in solving large deformation problems and are compared with the experimental data in literature (Section 4). Finally concluding remarks are made (Section 5).

2. SPH model design

In classical SPH, the mesh-free nature is attained by representing the domain with integral interpolant of arbitrarily distributed particles using kernel function [20]. The uniqueness of SPH method is that it is not affected by the arbitrarily distributed particles. The particles in SPH domain have no connectivity between them and possess their individual material characteristics. Although the mesh-free nature is attained, the problem is the stability. This stability is then provided by the kernel approximation which is the integral representation of the function. As the integral interpolant does not give good approximation of derivatives near boundaries, the least squares approximation method is used in this paper.

This function is then approximated by the particles called particle approximation which involves the summation of neighboring particles of the support domain. The compact supportedness property of the function is attained at this stage. Even though the particle approximation at each time step ensures adaptive nature of SPH, care should be taken in choosing the time stepping scheme. The PDEs are discretized into ODEs after the particle approximation and then the ODEs are solved using numerical techniques explicitly.

2.1. SPH equations of motion

In this paper, Lagrangian form of the Navier Stokes equation is used as the governing equations for free surface viscous flows. In an open boundary domain Ω with boundary Γ, let ρ, υ, μ and p be the density, velocity, dynamic viscosity and pressure fields representing the state variables. The Lagrangian form of conservation equations of mass and momentum for weakly compressible viscous flow is as [35]:

$$\frac{D\rho}{Dt} = -\rho\ \nabla.\upsilon, \tag{1}$$

$$\rho\ \frac{D\upsilon}{Dt} = -\nabla p + \nabla.(\mu\ \sigma) + g, \tag{2}$$

The system Eqs. (1)–(2) is closed by the Tait's equation of state as [4,17]:

$$p(\rho) = \frac{\rho_0\ c_0^2}{\gamma}\left(\left(\frac{\rho}{\rho_0}^{\gamma}\right) - 1\right), \tag{3}$$

where c_0 is the speed of sound, which reduces the density fluctuation, takes the value of 20 in this work and γ taking the value of 7.

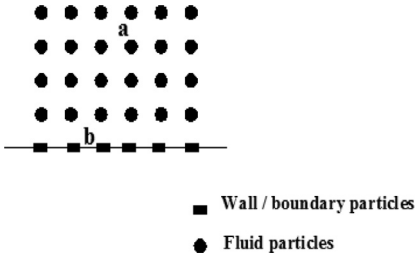

Fig. 1. Sketch showing solid boundary.

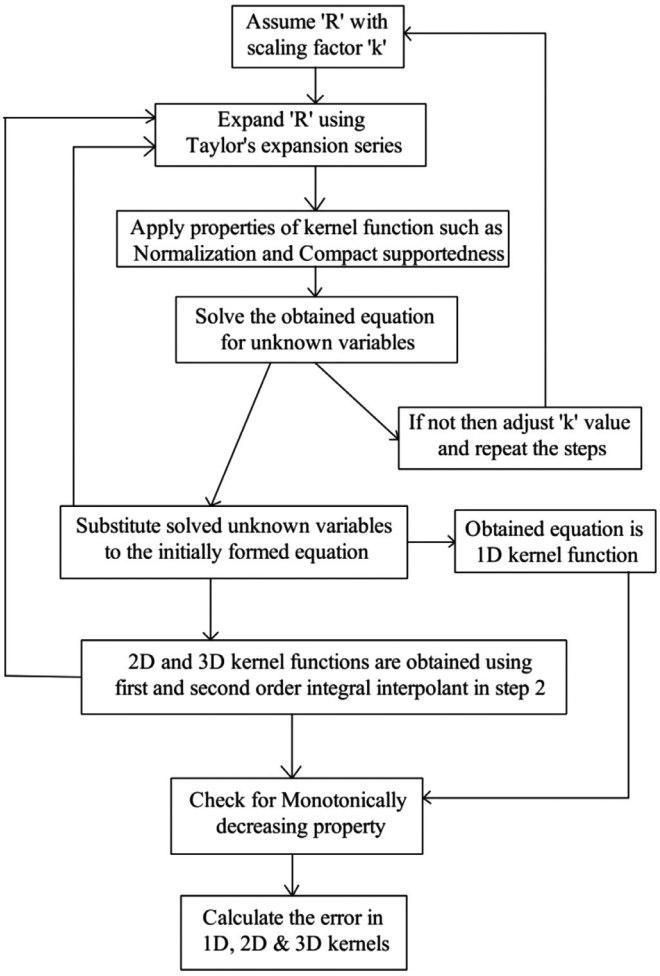

Fig. 2. flowchart for deriving a new kernel function.

The Eq. (3) acts as the incompressibility constraint i.e., the WCSPH (Weakly Compressible SPH) approach where pressure is an explicit function of density, the solution of matrix equation is obtained for each time step and the pressure field of water flow gives the approximated value.

The turbulence model by Large Eddy Simulation (LES) framework [34] is used here for studying dam break phenomena with breaking waves. For free fluid, the continuity and momentum equation in 3D in dimensional form is:

$$\nabla . u_f = 0, \tag{4}$$

$$\frac{Du_f}{Dt} = -\frac{1}{\rho_w}\nabla p + \gamma_w \nabla^2 u_f + g + \frac{1}{\rho_w}\nabla . \tau, \tag{5}$$

where u_f, ρ_w, γ_w, p and τ are the velocity vector of free fluid, density, kinematic viscosity, fluid pressure and turbulence stress

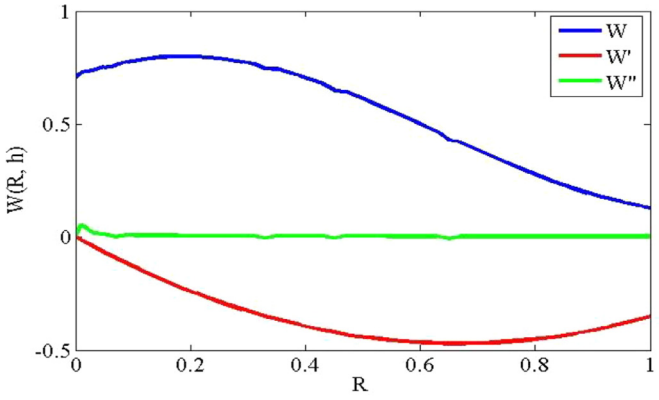

Fig. 3. Inverse Logarithmic kernel function and its derivatives.

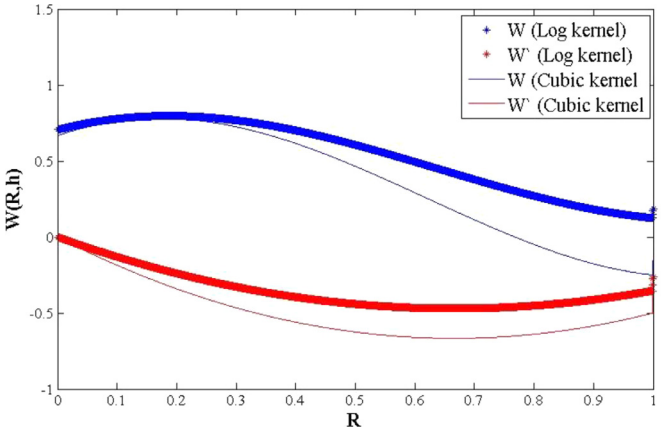

Fig. 4. Comparison of inverse logarithmic kernel function with cubic spline.

respectively. The turbulence stress is modeled using LES method [36] as:

$$\frac{\tau_{IJ}}{\rho_w} = 2\vartheta_T S_{IJ} - \frac{2}{3}\, k.\delta_{IJ}, \tag{6}$$

where τ_{IJ}, ρ_w, υ_T, S_{IJ}, k and δ_{IJ} are the turbulence stress, density, turbulence eddy viscosity, strain rate of mean flow, kinetic energy and Kronecker delta function respectively. Here, the eddy viscosity assumption [36] is used to model the sub-particle scale turbulence stress tensor.

$$\vartheta_T = (C_s \Delta)^2 \left|\vec{S}\right|, \tag{7}$$

where C_s is the Smagorinsky constant and it is taken the value of 0.2 and $|\vec{S}|$ is the local strain rate which is equal to $(2.S_{IJ}.S_{IJ})^{1/2}$. The turbulent eddy stress becomes zero near the solid boundary wall.

2.2. LSQ based SPH approach

The least squares method has been used to approximate the derivatives of the function rather than using integral interpolant which does not give good approximation of functional derivatives near the boundary particles [35,37]. The LSQ based functional f(t, $\vec{x}$) approximation and its first (f_k) and second (f_{kl}) derivatives are as [37,38]:

$$f_h(t,\vec{x}) = \Pi f_h(t,\ \vec{x}) = \sum_{i=1}^{N} f_i(t)\ \varphi\left(\vec{x_i},\ \vec{x}\right), \tag{8}$$

$$f_{kh}(t,\vec{x};\ \vec{z}) = \Pi_k f_h(t,\ \vec{x}) = \sum_{i=1}^{N} f_i(t)\ \eta_k\left(\vec{x_i},\ \vec{x}\right), \tag{9}$$

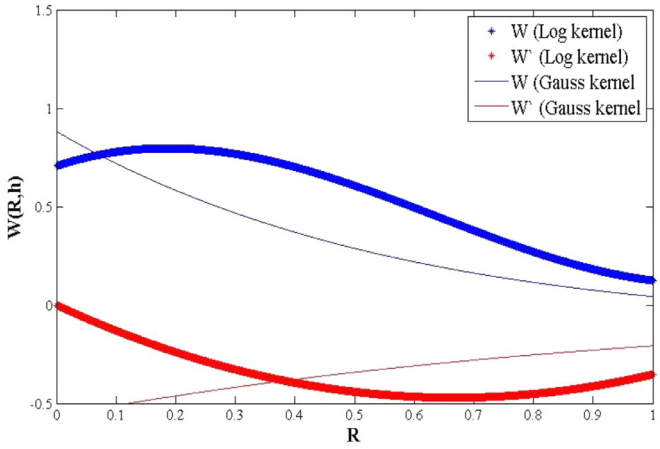

Fig. 5. Comparison of inverse logarithmic kernel function with gauss kernel.

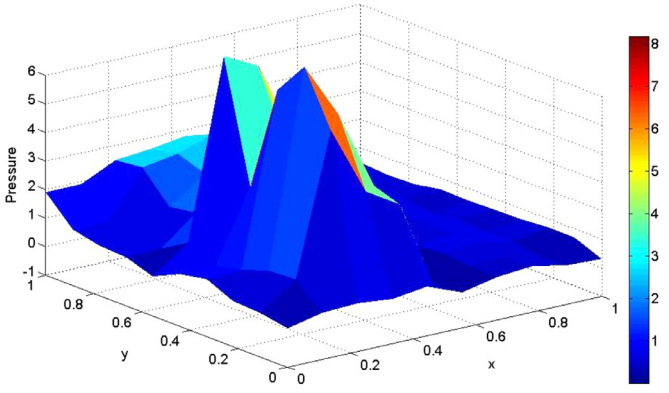

Fig. 6. 2D shock wave propagation using inverse log kernel - Pressure profile at 1 s.

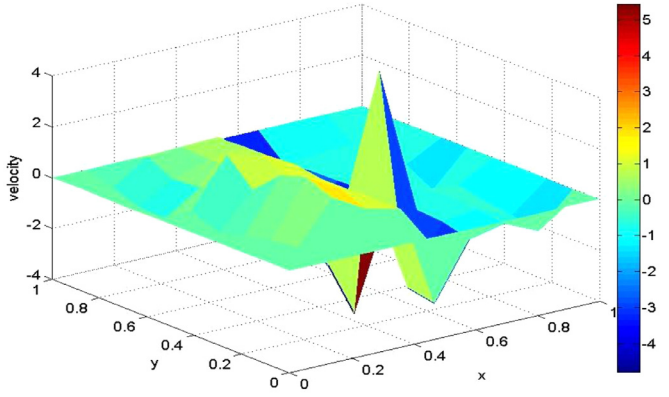

Fig. 7. 2D shock wave propagation using inverse log kernel - Velocity profile at 1 s.

$$f_{klh}(t,\vec{x};\ \vec{z}) = \ \Pi_{lk} f_h(t,\ \vec{x}) = \ \sum_{i=1}^{N} f_i(t)\ \psi_{kl}\left(\vec{x_i},\ \vec{x}\right), \tag{10}$$

where Π, Π_k and Π_{lk} are the functions and their derivatives as a linear combination of the neighbouring points for k and l values 1, 2 and 3. Using the least squares approximation, the functions Φ, η_k and ψ_{kl} are computed at each point. The least square approximation system is then applied to Eqs. (1) to (3) at the point $\vec{x_i}$ as [35]:

$$\frac{D\Pi_\rho\left(t,\ \vec{x_i}\right)}{Dt} = \ -\Pi\ \rho\left(t,\ \vec{x_i}\right)\ \nabla.\Pi\vec{v}\left(t,\ \vec{x_i}\right), \tag{11}$$

$$\Pi\rho\left(t,\ \vec{x_i}\right)\frac{D\Pi\vec{\vartheta}\left(t,\vec{x_i}\right)}{Dt} = \ -\nabla\Pi\ \rho\left(t,\ \vec{x_i}\right)\ +\ \mu\nabla.\Pi\sigma\left(t,\ \vec{x_i}\right), \tag{12}$$

$$\Pi_\rho\left(t,\vec{x_i}\right) = \left(\frac{\rho}{\rho_0}^{\gamma} - 1\right)\Pi\rho_0\ \left(t,\ \vec{x_i}\right)\ \Pi\frac{c_0^2}{\gamma}\left(t,\ \vec{x_i}\right), \tag{13}$$

for all i ranging from 1, 2 ..... N. After applying the properties of operator Π, the system of Eqs. (11–13) can be rewritten as:

$$\frac{D\rho_i(t)}{Dt} = \ -\rho_i\ (t)\ \Pi\ \nabla.\vec{v}\left(t,\ \vec{x_i}\right), \tag{14}$$

$$\rho_i(t)\ \frac{D\vec{\vartheta}_i(t)}{Dt} = \ -\Pi\ \nabla\rho\left(t,\ \vec{x_i}\right)\ +\ \mu\ \Pi\ \nabla.\sigma\ \left(t,\ \vec{x_i}\right), \tag{15}$$

$$p_i(t) = \left(\frac{\rho}{\rho_0}^{\gamma} - 1\right)\rho_i(t)\ \frac{c_i^2}{\gamma}(t), \tag{16}$$

These partial derivatives Eqs. (14) to (16) are then reduced to a series of time dependent system of ordinary differential equations which are then solved using time integration scheme.

2.3. Treatment of boundary condition

The solid boundaries in SPH are modeled by assigning wall / virtual particles that is used to treat the solid boundary conditions [5]. The properties such as density and pressure of the ghost particles are similar to that of the corresponding virtual particles but possess opposite velocity. Also, the virtual particles at the boundary possess sufficient repulsive boundary force that helps to reflect the inside the domain when the particle approaches the boundary. The position of boundary particles remains fixed irrespective of the moving solid boundary as shown in Fig. 1.

The equation describing the force applied pair wise along the centerline of the real and virtual particles is shown below:

$$PB_{ij} = \begin{cases} D\left[\left(\frac{r_0}{r_{ij}}\right)^{n_1} - \left(\frac{r_0}{r_{ij}}\right)^{n_2}\right] & \left(\frac{r_0}{r_{ij}}\right) \le 1 \\ 0 & \left(\frac{r_0}{r_{ij}}\right) > 1, \end{cases} \tag{17}$$

where the parameters n_1 and n_2 are taken as 12, and 4 respectively and r_0 is the cut-off distance. If the cut off distance is too large, more repulsive force is felt on some particles and leads to initial disturbance and blow up of particle positions and if the cut off distance is too small, the real particles already penetrate the boundary before the influence of repulsive force. Hence to avoid this issue, the cut off distance is chosen close to the initial particle spacing.

3. Kernel function for SPH

The first step in the integral representation of an arbitrary function is the kernel smoothing function. It starts from the delta-dirac distribution given by [14]:

$$f(x) = \int^{f} (x').\delta\left(x - x'\right)dx', \tag{18}$$

In Eq. (18), δ is replaced by a kernel weight function, W and the equation becomes [20]:

$$f(x) = \int^{f} \left(x'\right).\ W\left(x - x'\right)dx', \tag{19}$$

In Eq. (19), f (x') denotes the arbitrary function of an arbitrary particle x' and W (x – x') denotes the smoothing kernel function. By representing the domain with arbitrarily distributed particles, the mesh-free nature is attained, but the stability of the domain is

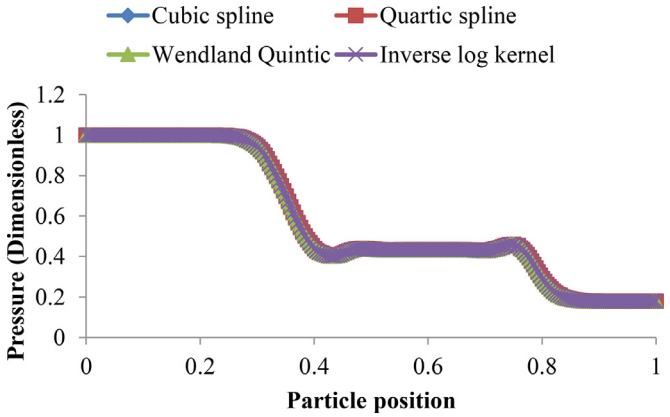

Fig. 8. Pressure plot at various particle position.

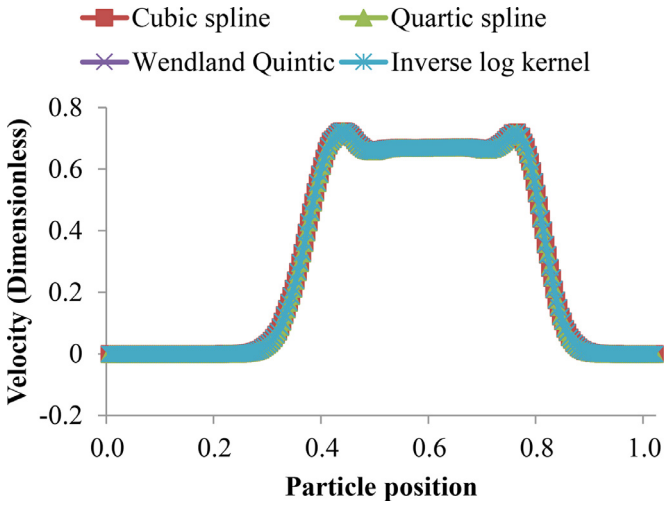

Fig. 9. Velocity profile at various particle positions.

not accounted for. This stability is then corrected by applying weak form formulation in function approximation i.e., integral representation of the function. The function approximation involves approximate functional form implicitly from a finite set of data points. Taylor's expansion series in then applied to function approximation (Eq. (10)) which includes the data of neighboring particles (i.e., local information of a particle). This field function approximation is collectively known as the Kernel function in SPH.

$$f(x') = f(x) + f'(x)(x - x') + \frac{1}{2}f''(x)(x - x')^2 + \ldots, \tag{20}$$

The Eq. (20) can be rewritten as [14]:

$$\langle f(x)\rangle = \sum_{k=0}^{n} A_k f^{(k)}(x) + r_n\left(\frac{x - x'}{h}\right), \tag{21}$$

From Eq. (21), the moments can be arrived as mentioned by [14],

$$M_0 = \int_{\Omega} W\ (x - x',\ h)dx' = 1, \tag{22}$$

$$M_1 = \int_{\Omega} (x - x').\ W\ (x - x',\ h)dx' = 0, \tag{23}$$

$$M_2 = \int_{\Omega} (x - x')^2.\ W\ (x - x',\ h)dx' = 0, \tag{24}$$

$$M_n = \int_{\Omega} (x - x')^n.\ W\ (x - x',\ h)dx' = 0, \tag{25}$$

These equations from (22) to (25) form the moment conditions for deriving a new smoothing kernel function. As the accuracy and consistency of the SPH method in continuous form is based on the Kernel function, it plays a vital role in the computational domain. Significant research works were carried out to determine the most appropriate kernel function for hydrodynamic problems. It was stated in some works that cubic spline performs better than any other kernel functions [18] where the spline in the polynomial form avoids the problem of Runge phenomenon i.e., divergent approximation due to interpolation and the problem of oscillation at the edge of interval. However, according to Weierstrass approximation theorem, high degree polynomial can result in oscillation at the edge of interval. The main disadvantage of these polynomial functions say cubic or quintic or quartic, is that they are not continuous i.e., they are piece-wise polynomial functions. Hence some authors carried research to formulate a new continuous kernel function in polynomial form [22,23].

The key properties of the kernel functions [39] are normalization, compact supportedness, monotonically decreasing function, satisfying delta-dirac condition, even function and smoothness. The compact supportedness property of a function defines the spread of a specific smoothing function. This compactness property within a compact set represents the transformation of a function from global to local coordinate system of matrices. The monotonically decreasing property of a function is regarded as the distribution or measure of the function. The flowchart of the methodology for deriving a new kernel function is shown in Fig. 2.

By using the above conditions, a new kernel function is formulated which is also known as the inverse logarithmic kernel function as it is derived from inverse function. The scaling factor used for deriving the inverse log kernel function is 2. The inverse log

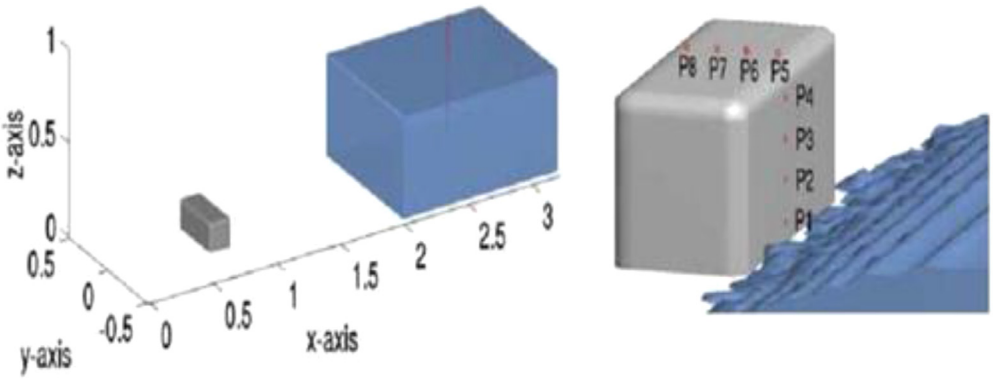

Fig. 10. Image showing dam break experimental setup and the measurement points for pressure (P) [1].

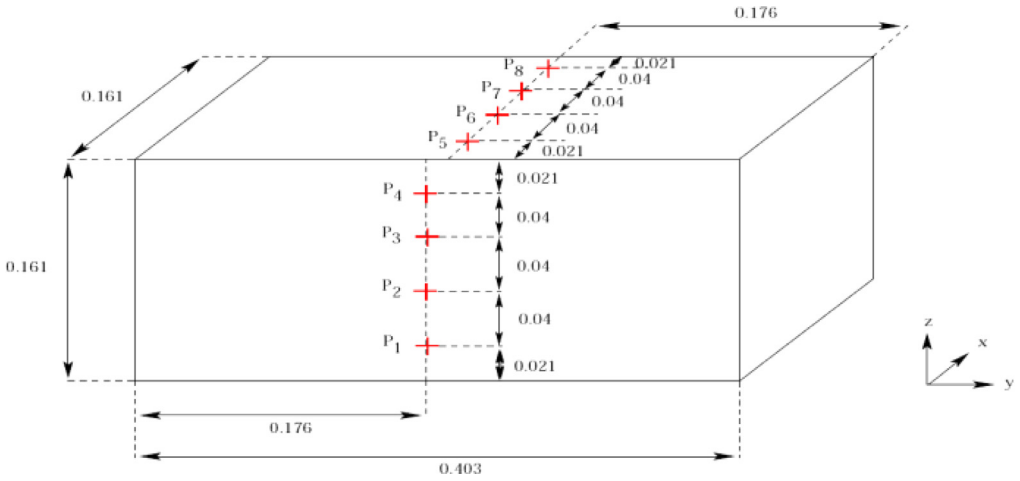

Fig. 11. Description of the box for pressure measurement [1].

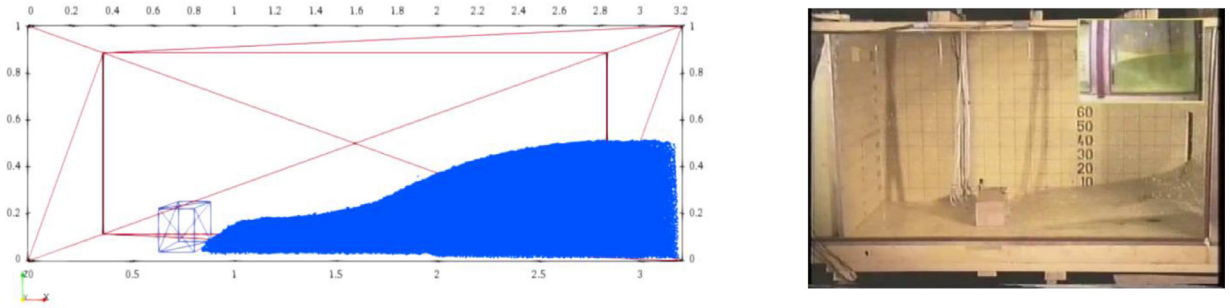

Fig. 12. 3D visualization of SPH model compared with the experiment at $t = 0.4$ s [1].

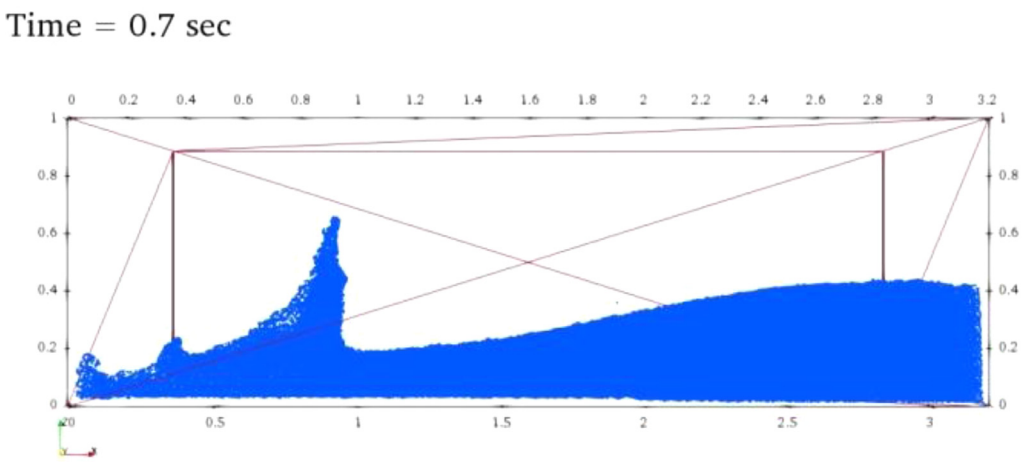

Fig. 13. 3D visualization of SPH dam break model at $t = 0.7$ s.

kernel function constructed is shown below in Eq. (26):

$$W(x - x',\ h) = W\ (R,\ h) = \alpha_d \begin{cases} \left[2 - 2R^2 + R^3\right], & 0 \le R \le 1 \\ 0, & R > 1 \end{cases} \tag{26}$$

where $R = r$ / h, r is the relative distance between two particles, α_d is the normalized coefficient in d dimensional space having the values of:

$$\alpha_1 = \frac{6}{17\ h};\ \alpha_2 = \frac{12}{29\pi h^3};\ \alpha_3 = \frac{9}{29\pi h^3}$$

in one, two and three dimensional space respectively. The inverse logarithmic kernel function and its derivatives are marked in the Fig. 3.

It is important to note that the inverse log kernel function curve shows smooth continuous curve with non-negativity and satisfies normalization condition. The blue line indicating the kernel function curve shows that the function converges to zero as R increases and this is valid only in the prescribed limit else the equation becomes invalid. A high center peak value of 4/5 for the new inverse log kernel was found which is higher than that of cubic spline function from which, we can conclude that high accuracy in particle approximation is yielded by the new kernel. The one particular characteristic that is particularly pertinent is

the compact supportedness which is illustrated in Fig. 3 where the first derivative of the function crosses x and y axis exactly at zero intercept. The second derivative of the kernel function marks a straight line in the plot ensuring zero error in the approximation which is a notable feature of this study. It is worth to mention that the first moment of the smoothing function is calculated to be zero that signifies the symmetricity of the new kernel function.

The error is estimated from the second moment equation (Eq. (24)) by expanding the moment equation using Taylor's series. In the new inverse logarithmic kernel function, the error is obtained around 0.035 h^2 which indicates very less error nearing zero whereas the existing cubic spline function, Gaussian function and double cosine function show error of $3h^2$, h^2 and $0.6h^2$ respectively [31]. Since the second momentum of the function is solved, this can be reproduced for n^{th} order polynomial which marks the higher order consistency. The superiority of the inverse logarithmic kernel function is illustrated and compared with the cubic spline (Fig. 4) and Gaussian kernel function (Fig. 5). This diagram (Fig. 4) states that the inverse log kernel function is very close to the cubic spline function that are widely used in the simulation of hydrodynamic problems. The center peak value of the inverse log kernel (4/5) is significantly higher in comparison to the existing cubic spline which is ¾. The most important part of the kernel function is the determination of particles' contribution in the approximation process which is based on the center peak value of the kernel function [20]. A higher value of center peak value indicates an increase in particle contribution in the simulation. Likewise, inverse log kernel shows 80% of particle's contribution which is slightly higher than the cubic spline having 75%. On comparing with Gauss kernel, the center peak value of inverse log kernel is much higher and is also non-negative in the support domain. The second derivative of the Gauss kernel is also much higher than that of the inverse log kernel and hence we can state that inverse log kernel yields higher accuracy compared to Gauss kernel.

4. Numerical tests

The limitations of grid based methods show a great influence in solving hydrodynamic problems such as shock and high velocity impact as there exists large deformation and in-homogeneities in these problems. Therefore, in this paper, the proposed new SPH scheme is tested for the cases of 2D shock wave propagation and 3D dam break free surface flow simulation.

4.1. 2D shock wave propagation

The shock wave propagation problem is chosen as the numerical test as it can be stated as the best benchmark validation for large deformation problems. The Lagrangian form of the compressible Navier – Stokes equation for shock wave propagation is written in addition to Eq. (4) and (5) as [35]:

$$\alpha_1 = \frac{6}{17\ h};\ \alpha_2 = \frac{12}{29\pi h^3};\ \alpha_3 = \frac{9}{29\pi h^3}$$

The governing Eqs. (4, 5 & 27) are then solved with appropriate boundary conditions. Here, we set μ and k to be zero, so that the solutions of Eq. (1–3) tend to be the solutions of compressible Euler equation. The indeterminate system of matrix generated is here counter forted by the equation of state from the theory of gas dynamics as:

$$p = (\gamma - 1)\rho E, \tag{28}$$

The value of gamma is taken as 1.4. Now these equations are solved numerically and the plot of pressure and velocity profile at 1 second is shown in the Fig. 6 and 7.

At a time period of 1.865 second and a particle position of 0.004, the shock wave attains a maximum pressure of 1.008948 with the corresponding velocity as 0.00034 units. Similarly, the maximum velocity of 1.290458 is attained at a particle position 0.50533 & time period of 0.005 second and their corresponding pressure is 0.483709. Based on the analytical result obtained, it is evident that the pressure and velocity profiles discontinuous and linear whereas, in real-time, the discontinuities cannot be linear. The purpose of the numerical simulation is to capture the discontinuities in the shock wave precisely. This discontinuities of the shock waves are precisely plotted using four kernel functions namely inverse log kernel, cubic spline, quartic spline and Wendland quintic. The pressure and velocity distribution plot of 4 kernel functions are schematically shown in Fig. 8 and 9 respectively. The error estimated using analytical result with respect to the numerical one in calculating the pressure and velocity was 0.89% and 0.904% respectively. The relative percentage of error estimated for the four kernels are listed in Table 1. The error percentage is too high for quartic spline function. It was found that the proposed new kernel function achieved lesser error and surpasses the earlier work in this area in terms of accuracy of the SPH model.

Table 1
Table showing percentage of relative error in different kernel functions.

S. No	Kernel Function	Relative error (%)	
		Pressure	Velocity
1	Cubic Spline Kernel	0.91	0.909
2	Quartic Spline Kernel	0.915	0.91
3	Wendland Quintic Kernel	0.909	0.908
4	Inverse Logarithmic Kernel	0.89	0.904

4.2. 3D dam break flow against a cuboidal obstacle

This section provides an extensive validation of the proposed new SPH scheme with a standard dam break phenomenon as the characteristics of tsunami waves are closely represented by a broken dam-break wave front [40]. The numerical output from the 3D dam break phenomenon against a cuboidal obstacle are well validated against the published data in the literature [1]. The diagram of the experimental model setup described is shown in Fig. 10. The SPH tank dimension is 3.22 m × 1 m × 1 m, and the water column of 0.55 m height is stored on the right side of the model setup. The total simulation time is 6 s. The acceleration due to gravity g and the density of the fluid considered for the simulation are $-9.81\ m/s^2$ and $1000\ kg/m^3$ respectively. The CFL number considered in this simulation is 0.2. The interaction kernels used in this numerical model are inverse logarithmic kernel and Cubic spline kernel. This helps us to compare the efficiency of the proposed kernel over the existing function. The artificial viscosity formulation for SPH is considered having viscosity value (α) equal to 0.015. The bottom profile of the SPH model is considered as horizontal dry bed.

The position of pressure transducers (P1, P2, P3, P4, P5, P6, P7 & P8) for measuring the pressure evolution is shown in Fig. 11. The inter–particle distance of the model considered for both the numerical cases is dx = 0.012 m. The total particle involved in the simulation was 491,419 particles consisting of 105,653 boundary particles and 385,766 fluid particles. The processor used for the simulation is Intel®Core™i5–7400UCPU@3.00 GHz, 8.0GB RAM memory, 64 bit operating system and 2GB graphic card.

In Fig. 12, the 3D simulation results of the SPH model are compared with the experimental result at time period 0.4 s and another image visualizing the SPH model at t-=0.7 s is shown in Fig. 13. Once the flaps are removed, the water stored behind the reservoir flows towards the obstacle in the left side of the setup. As the water hits the obstacle at t = 0.44 s, the height grows rapidly

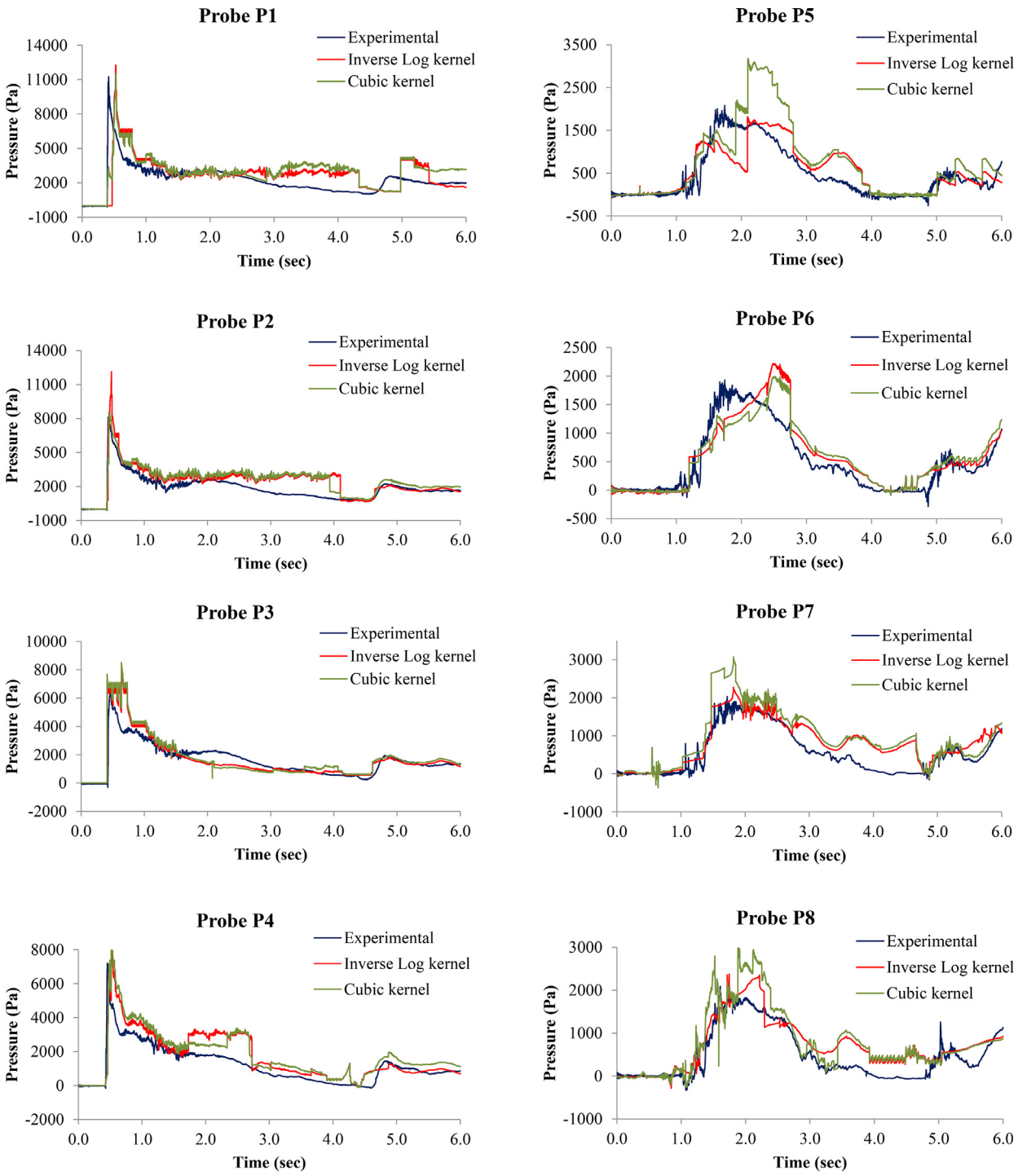

Fig. 14. Pressure evolution for the flow at probe P1 to P8 [1].

and hence the vertical height of the water column rises rapidly. The pressure plot for probes P1 to P4 shows that the pressure rises rapidly during time period of 0.44 s to 0.5 s.

The numerical and experimental comparisons of pressure plot for probe locations P1 to P8 are shown in Fig. 14. At $t = 0.7$ s, the water column reaches its maximum height and then the height decreases once the energy is dissipated. The water flows around the tank over a period of time. Due to gravity, the water segment subsides and transmits along the even dry bed. At 0.4 ⟨T⟩ 1.5 second, high pressure fluctuation of the numerical values are observed. During 3 to 6 s, the changing trend of the plot for all the results are the same. The high pressure fluctuations of the experimental values are due to the dynamic response of the pressure transducers. The average percentages of relative error in numerical simulation using inverse log kernel function for probes P1 to P8 are 5.06%, 6.16%, 0.58%, 4.79%, 0.67%, 0.77%, 2.63% and 2.27% respectively. Similarly, the relative error for Cubic spline kernel is shown in Table 2. From the table, it is clearly understood that inverse log kernel is capable of predicting particle properties accurately and better than cubic kernel. The cost effectiveness of the model is analyzed by comparing the computational cost of both the kernel functions. Computationally, the results are mixed as in

Table 2
Comparison of computational cost between two kernel functions & its relative error.

Probes (P1 to P8)	Computational cost (hours)		Relative error (%)	
	Cubic kernel	Inverse Log kernel	Cubic kernel	Inverse Log kernel
P1	6.81	6.80	6.24	5.06
P2	6.54	6.56	6.68	6.16
P3	7.11	7.07	2.04	0.58
P4	6.05	5.99	4.88	4.79
P5	6.55	6.62	1.57	0.67
P6	7.97	8.07	1.35	0.77
P7	8.015	7.86	3.58	2.63
P8	7.44	7.37	3.23	2.27

some cases inverse log kernel shows less cost and for some cases cubic kernel shows less cost. In this work, the influences of air, their interaction with the fluid particles are neglected and hence we could see a slight difference in the pressure plot between experiment and numerical results. The difference can further be reduced by increasing the number of particles in the domain that finally leads to convergence of the simulation. However, increase in number particles, simultaneously increases the computational cost of the model. This is one of the conclusions that can be derived from this work. In short, a good agreement between the numerical and experimental results could be seen which indicates the accuracy and stability of the improved SPH approach using new kernel function.

5. Conclusion

In this study, we seek to develop a novel approach for SPH, with a goal of attaining higher accuracy of the model. In order to reach our objective, we developed a new kernel function for SPH method. The approach is tested for large deformation problems. The developed new kernel function is approximated using Moving Least Squares based technique. The new SPH method is tested and validated for 2D shock wave propagation and 3D dam break flow simulation. One of the most significant observations of this study is that the new kernel function shows second order approximation of $0.035h^2$ that is zero error in the simulation which is far superior than the already existing cubic spline, Gaussian and double cosine kernel function which show errors up to $3h^2$, h^2 and $0.6h^2$ respectively. A higher center peak value of our new kernel function indicates an increase in particle contribution in the simulation. The ability of our new kernel function in capturing the discontinuities is numerically precisely plotted using 2D shock wave propagation study. The pressure and velocity values are compared with 4 existing kernel functions and the result showed 0.89% and 0.904% of accuracy for pressure and velocity using the inverse log kernel.

In our experimental validation, we have found that this new approach achieves average relative error percentage of not more than 6.16%. The proposed approach marginally out performs the other approaches by higher accuracy and higher particle contribution to the simulation. This study further analyzed the computational cost of the new kernel with the existing cubic kernel. Our most interesting finding is that mixed results were noted in the computational cost between the two kernel functions. Future research should therefore be taken to address the issue of reduction of computational cost of the approach. However, in summary, this work best offers the advantage of better accuracy and stability of the SPH method by proposing a new kernel function.

Declaration of Competing Interest

The author declare that they have no known competing financial interests or personal relations that could have appeared to influence the work reported in this paper.

The author states that they have no conflict of interest.

I, the undersigned declare that this manuscript is original, has not been published before and is not currently being considered for publication elsewhere.

I confirm that the manuscript has been read and approved by all named authors and that there are no other persons who satisfied the criteria for authorship but are not listed.

I understand that the Corresponding Author is the sole contact for the Editorial process. He/she is responsible for communicating with the other authors about progress, submissions of revisions and final approval of proofs

Acknowledgment

The author is grateful to Dr.Sudarshan Tiwari, Fraunhofer Institut Techno- und Wirtschaftmathematik, Erwin-Schrõdinger-Strasse, Kaiserslautern, Germany for his helpful and valuable discussions

Funding

This study received no specific grant from any funding agency in the public, commercial, or not-for-profit sectors.

Data availability statement

Previously reported data were used to support this study and are available at the web link (https://spheric-sph.org/tests/test-2). These prior studies and datasets are cited at relevant places within the text as reference [1].

References

[1] K.M.T. Kleefsman, G. Fekken, B.B. Veldman, E.P. A, B. Iwanowski, J. Comput. Phys. 206 (2005) 363–393.
[2] L.B. Lucy, Astron. J. 82 (1977) 1013–1024.
[3] R.A. Gingold, J.J. Monaghan, Royal Astronomical Soc. (181) (1977) 375–389.
[4] J.J. Monaghan, Annu. Rev. Astron. Astrophys. 30 (1992) 543–574.
[5] J.J. Monaghan, J. Comput. Phys. 110 (2) (1994) 399–406.
[6] M. Yavuz, N. Sene, J. Ocean Eng. Sci. 6 (2) (2021) 196–205, doi:10.1016/j.joes.2020.10.004.
[7] T. Rabczuk, T. Belytschko, S.P. Xiao, Stable Particle Methods Based Lagrangian Kernels 193 (2004) 1035–1063.
[8] T. Belytschko, Y. Guo, W.K. Liu, S.P. Xiao, A Uniÿed Stability Anal. Meshless Particle Methods (July 1999) 1359–1400 2000.
[9] J.J. Monaghan, J.C. Lattanzio, Astron. Astrophys. 149 (1985) 135–143.
[10] J.J. Monaghan, H. Pongracic, Appl. Numerical Mathematics 1 (3) (1985) 187–194.
[11] J.P. Morris, J.J. Monaghan, J. Comput. Phys. 50 (136) (1997) 41–50.
[12] J.J. Monaghan, Comput. Phys. Commun. 48 (1988) 89–96.
[13] J.J. Monaghan, R.A. Gingold, J. Comput. Phys. 52 (2) (1983) 374–389.

[14] M.B. Liu, G.R. Liu, Arch. Comput. Methods Eng. 17 (1) (2010) 25–76.
[15] M. Sasson, S. Chai, G. Beck, Y. Jin, J. Rafieshahraki, J. Ocean Eng. Science 1 (2) (2016) 119–128, doi:10.1016/j.joes.2016.03.004.
[16] M.M. Mousa, J. Ocean Eng. Sci. 3 (4) (2018) 303–309, doi:10.1016/j.joes.2018.10.006.
[17] P.W. Randles, L.D. Libersky, Comput Methods Appl. Mech. Eng. 7825 (139) (1996) 375–408.
[18] D.A. Fulk, D.W. Quinn, J. Comput. Phys. 180 (126) (1996) 165–180.
[19] W. Swegle, S.W. Attaway, Comput. Mech. 17 (1995) 151–168.
[20] M.B. Liu, G.R. Liu, K.Y. Lam, Z. Zong, Comput. Mech. 30 (2) (2003) 106–118.
[21] J. Ha, Mech.Unimelb.Edu.Au (December) (2004).
[22] J. Hongbin, D. Xin, J. Comput. Phys. 202 (2005) 699–709.
[23] R.M. Cabezón, D. García-senz, A. Relaño, J. Comput. Phys. 227 (2008) 8523–8540.
[24] H. Ahmad, T.A. Khan, P.S. Stanimirović, Y.M. Chu, I. Ahmad, Complexity 2020 (2020) 1–14, doi:10.1155/2020/8841718.
[25] H. Ahmad, T.A. Khan, J. Low Frequency Noise Vibrat. Active Control 38 (3–4) (2019) 1113–1124.
[26] H. Ahmad, T.A. Khan, C. Cesarano, Axioms 8 (4) (2019) 1–16.
[27] H. Ahmad, A.R. Seadawy, T.A. Khan, Math. Comput. Simul 177 (2020) 13–23.
[28] H. Ahmad, T.A. Khan, I. Ahmad, P.S. Stanimirović, Y.M. Chu, Results Physics 19 (2020) 1–8.
[29] M. Inc, M.N. Khan, I. Ahmad, S.W. Yao, H. Ahmad, P. Thounthong, Results Physics 19 (2020) 1–6 August.
[30] K.K. Ali, A.R. Hadhoud, M.A. Shaalan, J. Ocean Eng. Sci. 3 (3) (2018) 237–243, doi:10.1016/j.joes.2018.07.001.
[31] X.F. Yang, S.L. Peng, M.B. Liu, Appl. Math. Model 38 (2014) 3822–3833.
[32] T.A. Sulaiman, H. Bulut, J. Ocean Eng. Sci. 4 (1) (2019) 1–6, doi:10.1016/j.joes.2018.12.001.
[33] L. Fang, J.C. Marongiu, J. Leduc, A. Amicarelli, J. Caro, Chin. J. Aeronaut. 30 (1) (2017) 1–14.
[34] G. Duan, B. Chen, Appl. Math. Model 39 (10–11) (2015) 3135–3149.
[35] S. Tiwari, Int. Series Numerical Math. 141 (2000) 1–12.
[36] J. Smagorinsky, Monthly Weather Review 91 (3) (1963) 99–164.
[37] Wing Kam Liu, Shaofan Li, Ted Belytschko, Comput. Methods Appl. Mech. Eng. 143 (1–2) (1997) 113–154.
[38] R. Salehi, M. Dehghan, J. Comput. Appl. Math. 249 (2013) 120–132.
[39] M.B. Liu, G.R. Liu, K.Y. Lam, Z. Zong, Shock Waves 12 (6) (2003) 509–520.
[40] Hubert Chanson, Coastal Eng. J. 48 (4) (2006) 355–370.